



Synthesis, crystal structures and two-photon absorption properties of a series of terpyridine-based chromophores

Bing Liu^a, Qiong Zhang^a, Hongjuan Ding^c, Guiju Hu^a, Yajun Du^a, Chuankui Wang^c, Jieying Wu^a, Shengli Li^a, Hongping Zhou^a, Jiayang Yang^a, Yupeng Tian^{a,b,d,*}

^a Department of Chemistry, Key Laboratory of Functional Inorganic Material Chemistry of Anhui Province, Anhui University, 230039 Hefei, PR China

^b State Key Laboratory of Crystal Materials, Shandong University, 250100 Jinan, PR China

^c Department of Physics, Shandong Normal University, Jinan 250014, PR China

^d State Key Laboratory of Coordination Chemistry, Nanjing University, 210093 Nanjing, PR China

ARTICLE INFO

Article history:

Received 12 January 2012

Received in revised form

18 March 2012

Accepted 19 March 2012

Available online 29 March 2012

Keywords:

Terpyridine derivatives

Synthesis

Single-photon-excited fluorescence

Two-photon-excited fluorescence

Photophysical properties

Density functional theory

ABSTRACT

A series of 2, 2': 6', 2''-terpyridine-based chromophores (**L1**, **L2**, **L3** and **L4**) with intramolecular 'push–pull' structure have been designed and synthesized. The single crystals of **L1**, **L2** and **L4** were obtained and solved by X-ray diffraction analysis. The photophysical behavior and the connections between structure and properties of the chromophores were investigated both experimentally and theoretically. It is revealed that the chromophores exhibit sensitive single-photon-excited fluorescence emission with high quantum yields, strong two-photon-excited fluorescence and large two-photon absorption cross sections, especially in DMF solution. It was also found that methylformate units as a peripheral groups attached to the triphenylamine moiety influence the structures, photophysical properties of the chromophores obviously.

© 2012 Elsevier Ltd. All rights reserved.

1. Introduction

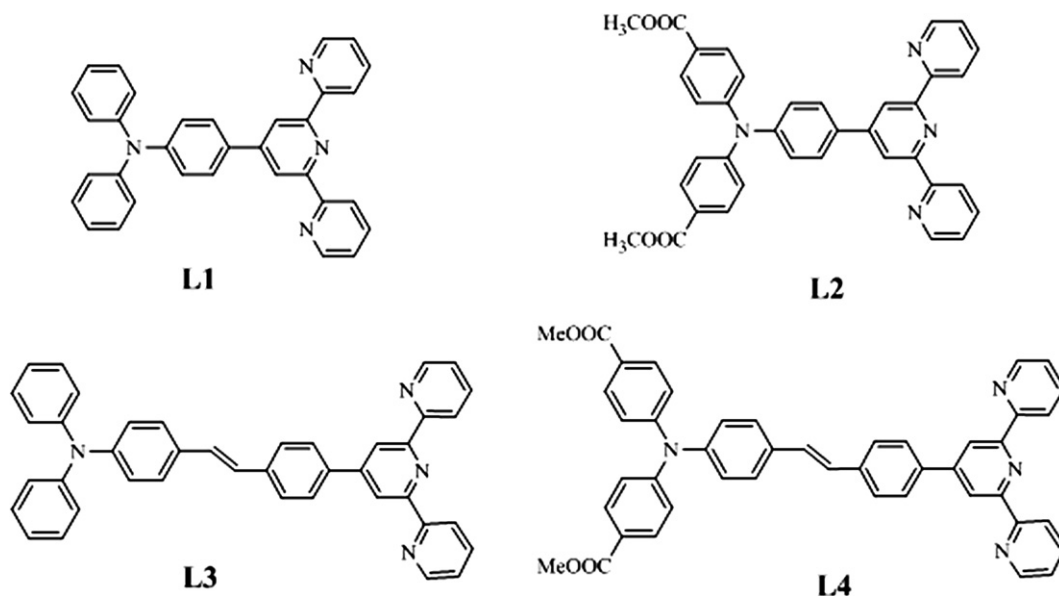
Recently, organic nonlinear optical materials [1,2] with striking two-photon absorption (TPA) effect and large TPA cross sections have attracted growing interest due to their potential applications in the areas of optical limiting [3–6], two-photon photodynamic therapy [7], multiphoton fluorescence microscopy [8–10], three-dimensional (3D) optical data storage [11–13], 3-D micro-fabrication [14–17]. These applications strongly depend on the large TPA cross sections of the specifically engineered organic molecules.

Therefore, many research groups have focused on designing and synthesizing new compounds exhibiting large TPA cross sections (δ_{TPA}) values in the field of functional materials. In recent publications, well-defined strategies have successfully been used to design organic molecules with large δ_{TPA} and high quantum yield (Φ). A variety of dipolar (donor-bridge-acceptor, D- π -A), quadrupolar (D- π -D, D- π -A- π -D, A- π -D- π -A), and multipolar chromophore

molecules were reported, and their structure-TPA properties were investigated [18–20]. However, apart from the high δ_{TPA} values, TPA chromophores have to satisfy various requirements for the specific purposes, such as excellent photostability, proper water solubility, and good biocompatibility. In this context, a series of terpyridine-based chromophores with TPA activity and coordinating abilities were designed, which is based on the following considerations: (1) 2, 2': 6', 2''-terpyridine and their structural analogs with rich coordination chemistry have been extensively studied for their high binding affinity toward a variety of transition as well as rare earth metal ions, giving rise to diverse metallo-supramolecular architectures, resulting in interest redox and photophysical properties [21–26]; (2) triphenylamine moiety having a strong electron donor and efficient π -electron bridge, along with vinyl group, as a building block has been used to develop TPA chromophores [27–29]; (3) methylformate group attached to the triphenylamine moiety is of potential coordinating group after its hydrolysis. So this design strategy combines those advantages to construct novel model terpyridine-based TPA chromophores shown in Scheme 1 (**L1**, **L2**, **L3** and **L4**). Herein, the synthesis and their photophysical properties of them were systematically investigated both experimentally and theoretically.

* Corresponding author. Department of Chemistry, Key Laboratory of Functional Inorganic Material Chemistry of Anhui Province, Anhui University, 230039 Hefei, PR China.

E-mail address: liubing3412@163.com (Y. Tian).



Scheme 1. Chemical structures of L1, L2, L3 and L4.

2. Experiments

2.1. Materials and apparatus

All chemicals used were of analytical grade. The solvents were purified by conventional methods. The ^1H NMR and ^{13}C NMR spectra recorded on at 25 °C using Bruker Avance 400 spectrometer were reported as parts per million (ppm) from TMS. Mass spectra were determined with a Micromass GCT-MS (EI source). IR spectra were recorded on NEXUS 870 (Nicolet) spectrophotometer in the 400–4000 cm^{-1} region using a powder sample on a KBr plate.

X-ray diffraction data of single crystals were collected on CCD diffractometer. The determination of unit cell parameters and data collections were performed with Mo- $\text{K}\alpha$ radiation ($\lambda = 0.71073 \text{ \AA}$). Unit cell dimensions were obtained with least-squares refinements, and all structures were solved by direct methods using SHELXS-97. The other non-hydrogen atoms were located in successive difference Fourier syntheses. The final refinement was performed by full-matrix least-squares methods with anisotropic thermal parameters for non-hydrogen atoms on F^2 . The hydrogen atoms were added theoretically and riding on the concerned atoms.

UV–vis absorption spectra were recorded on UV-265 spectrophotometer. Fluorescence measurements were performed using a Hitachi F-7000 fluorescence spectrophotometer.

2.2. Measurements

2.2.1. The fluorescence quantum yields (Φ)

The fluorescence quantum yields (Φ) were determined by using coumarin 307 as the reference according to the literature method [30]. Quantum yields were corrected as follows:

$$\Phi_s = \Phi_r \left(\frac{A_r \eta_s^2 D_s}{A_s \eta_r^2 D_r} \right)$$

Where the s and r indices designate the sample and reference samples, respectively, A is the absorbance at λ_{exc} , η is the average refractive index of the appropriate solution, and D is the integrated area under the corrected emission spectrum [31].

2.2.2. TPA cross-section (δ)

TPEF spectra were measured using femtosecond laser pulse and Ti: sapphire system (680–1080 nm, 80 MHz, 140 fs, Chameleon II) as the light source. All measurements were carried out in air at room temperature. TPA cross sections were measured using two-photon-induced fluorescence measurement technique. The TPA cross sections (δ) are determined by comparing their TPEF to that of fluorescein in different solvents, according to the following equation [32]:

$$\delta = \delta_{\text{ref}} \frac{\Phi_{\text{ref}} c_{\text{ref}} n_{\text{ref}} F}{\Phi c n F_{\text{ref}}}$$

Here, the subscripts ref stands for the reference molecule. δ is the TPA cross-section value, c is the concentration of solution, n is the refractive index of the solution, F is the TPEF integral intensities of the solution emitted at the exciting wavelength, and Φ is the fluorescence quantum yield. The δ_{ref} value of reference was taken from the literature [33].

2.2.3. Fluorescence lifetime

For time-resolved fluorescence measurements, the fluorescence signals were collimated and focused onto the entrance slit of a monochromator with the output plane equipped with a photomultiplier tube (HORIBA HuoroMax-4P). The decays were analyzed by 'least-squares'. The quality of the exponential fits was evaluated by the goodness of fit (χ^2).

2.3. Preparation

2.3.1. 4'-(4-(Diphenylamino)phenyl)-2,2':6',2''-terpyridine (L1)

L1 was synthesized according to literature method [34].

2.3.2. 4'-(4-(4-(Diphenylamino)phenyl)aldehyde)-2,2':6',2''-terpyridine (L)

L (1.50 g, 3 mmol) and DMF (1.00 g, 13.7 mmol) were mixed in an ice bath, and then a solution of POCl_3 (2.00 g, 13.0 mmol) was added into the mixture dropwise in 10 min, and refluxed for 12 h. After being cooled to room temperature, the mixture was poured into ice water, adjusted to pH = 8 with sodium hydroxide, and then

filtered. The solid was purified by silica gel chromatography column using petroleum/ethylacetate (5:1 v/v) as the eluent. Yellow solid product **1** was collected. Yield 62.5%. Mp: 80 °C $^1\text{H NMR}$ (CDCl_3 , 400 MHz): 9.83 (s, 1H), 8.72 (m, 6H), 8.01 (m, 4H), 7.80 (d, 2H), 7.52 (m, 4H), 7.29 (m, 5H), 7.05 (m, 2H). MS: m/z (%) = 504.20 (100). FT-IR (KBr, cm^{-1}): 3427, 3057, 2924, 2726, 1691, 1586, 1508, 1489, 1469, 1439, 1390, 1324, 1281, 1219, 1164, 1117, 1075, 1038, 991, 895, 824, 792, 742, 717, 697, 658, 623, 578, 527.

2.3.3. 4''',4''-(4'-(4-(Diphenylamino)phenyl)aldehyde)-2,2':6',2''-Terpyridine (**2**)

2 was synthesized reference to **1**. Brown solid product **2** was collected (yield 73.3%). $^1\text{H NMR}$ ($\text{DMSO}-d_6$, 400 MHz): 9.92 (s, 2H), 8.76 (t, 4H), 8.69 (d, 2H), 8.04 (d, 4H), 7.90 (d, 4H), 7.53 (t, 2H), 7.38 (d, 2H), 7.28 (d, 4H). MS: m/z (%) = 504.20 (100). FT-IR (KBr, cm^{-1}): 3464, 3060, 2919, 2850, 1714, 1546, 1508, 1474, 1434, 1365, 1321, 1179, 1111, 1069, 1015, 968, 834, 793, 769, 731, 702, 659, 637, 528.

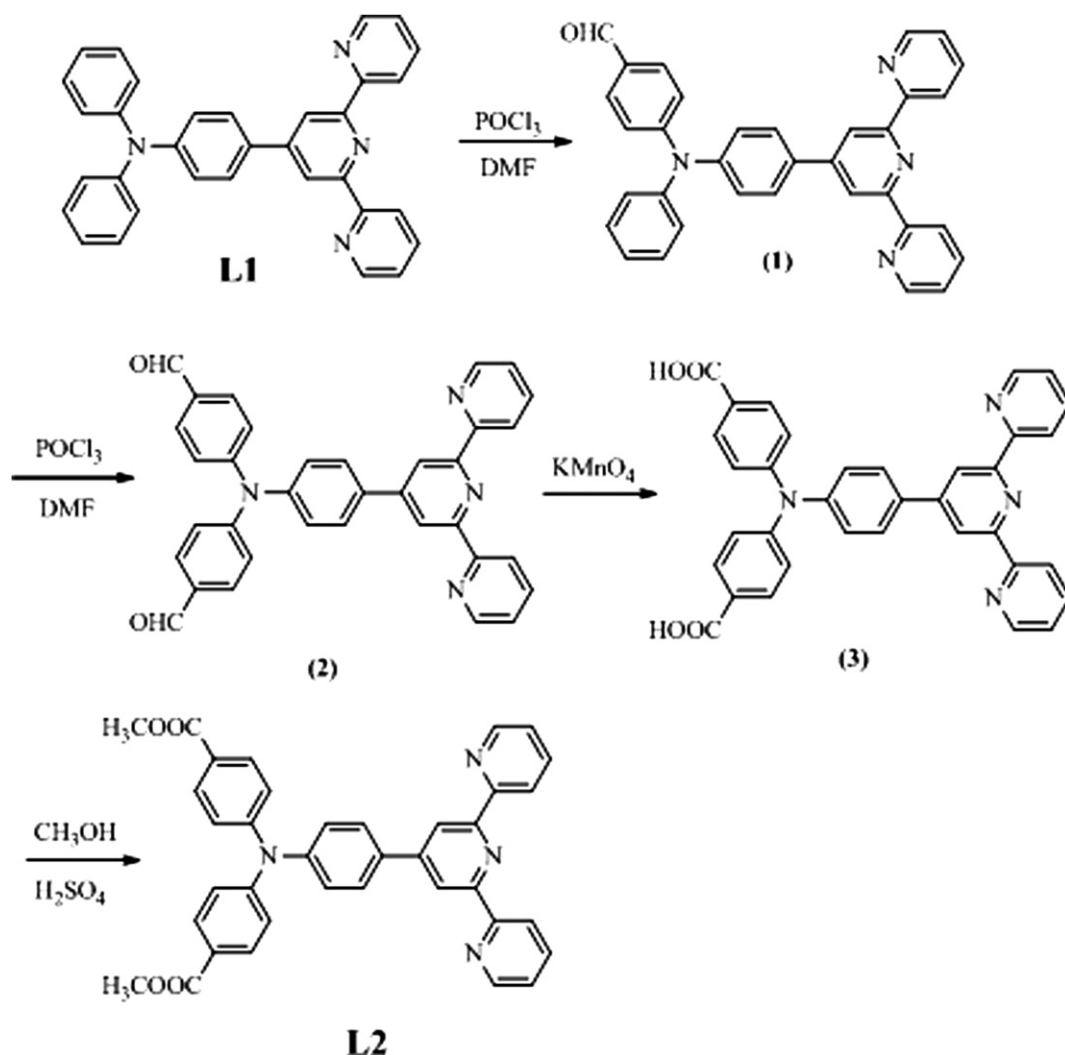
2.3.4. 4''',4''-(4'-(4-(Diphenylamino)phenyl)dibenzoic acid)-2,2':6',2''-terpyridine (**3**)

2 (1.00 g, 2 mmol) was dissolved in 150 mL of acetone, to which the aqueous solution 50 mL of KMnO_4 (1.26 g, 4 mmol) and K_2CO_3 (0.28 g, 2 mmol) were added slowly. The mixture was refluxed for

12 h, cooled and filtered. The filtrate was adjusted to pH = 1 with HCl, then filtered. The crude product was recrystallized from anhydrous ethanol to give 0.75 g yellow crystals **3** with yield 70.8%. Mp: 25 °C $^1\text{H NMR}$ ($\text{DMSO}-d_6$, 400 MHz): 8.81 (t, 6H), 8.18 (t, 2H), 8.03 (d, 2H), 7.92 (d, 4H), 7.65 (t, 2H), 7.33 (d, 2H), 7.18 (d, 4H).

2.3.5. 4'-(4-2-[dimethyl4,4'-(phenylazanediy) dibenzoate] phenyl)-2,2':6',2''-terpyridine (**L2**)

3 (0.75 g 1.32 mmol) was dissolved in 100 mL miscible liquids (methanol and H_2SO_4). The mixture was refluxed for 8 h. And then cooled to room temperature, the most methanol in the mixture was removed. The residue was dispersed in a large amount of water. The solution was adjusted to pH = 8 with K_2CO_3 and extracted three times with CH_2Cl_2 . The organic layer was dried over anhydrous MgSO_4 . The crude product was purified by silica gel chromatography column using petroleum/ethylacetate (15:1 v/v) as the eluent. Light yellow solid **L2** was collected. Yield 75.6%. Mp: 80 °C $^1\text{H NMR}$: (CDCl_3 , 400 MHz): 8.85 (s, 2H), 8.77 (d, 4H), 8.01 (q, 8H), 7.50 (t, 2H), 7.42 (d, 2H), 7.27 (d, 4H), 3.89 (s, 6H). $^{13}\text{C NMR}$ ($\text{DMSO}-d_6$, 100 MHz): 165.6, 155.6, 154.8, 150.2, 149.2, 148.5, 146.7, 137.5, 133.7, 130.9, 128.5, 126.2, 124.5, 124.1, 122.9, 120.9, 117.5, 51.9. Anal. Calcd. for $\text{C}_{37}\text{H}_{28}\text{N}_4\text{O}_4$: C, 74.95; H, 4.74; N, 9.39; O, 10.76%. Found: C, 74.99; H, 4.76; N, 9.45; O, 10.80%. MS: m/z (%) = 592.22 (100). FT-IR



Scheme 2. Synthesis route for **L2**.

(KBr, cm^{-1}): 3416, 3054, 2947, 1722, 1599, 1508, 1515, 1466, 1431, 1389, 1319, 1264, 1174, 1105, 1037, 1013, 990, 956, 892, 851, 792, 767, 737, 703, 659, 642, 623, 578, 523.

2.3.6. 4'-(4-{2-[4-(*N,N*-Diphenylamino)phenyl]ethenyl}phenyl)-2,2':6',2''-terpyridine (**L3**)

L3 was synthesized according to literature method [35].

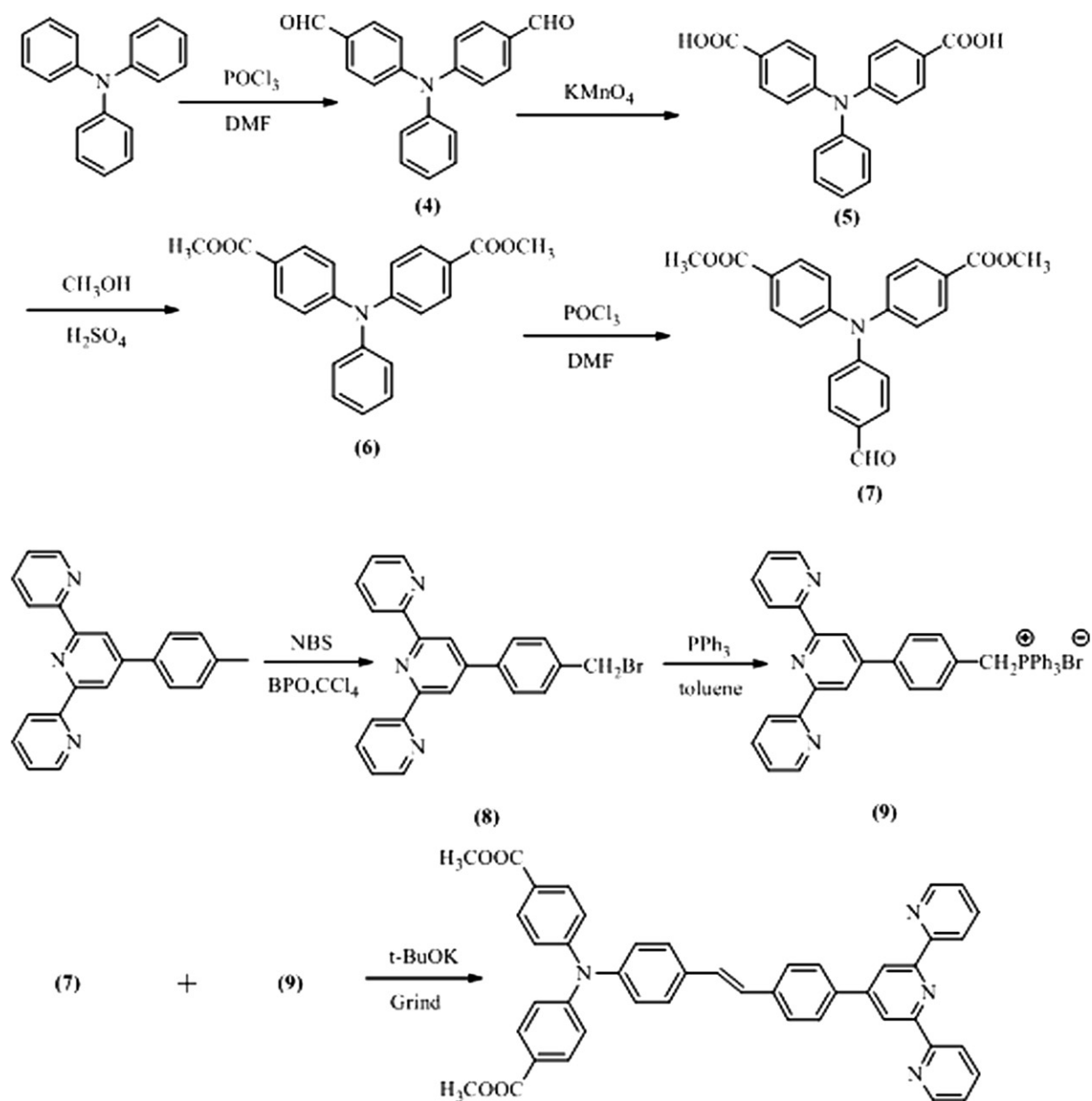
2.3.7. 4,4'-(phenylazanediyldibenzaldehyde (**4**)

Triphenylamine (12.20 g, 50 mmol) and DMF (37.00 g, 500 mmol) were mixed in ice bath and then POCl_3 (14.50 g, 100 mmol) was added dropwise within 10 min. The mixture was refluxed for 7 h, monitored by TLC. The mixture was cooled, poured into ice water, and then neutralized using saturated aqueous NaOH (adjust the pH > 8). The solution was extracted three times with

CH_2Cl_2 , and then dried using magnesium sulfate over night. The solvent was removed in vacuo. The residue was purified by flash column chromatography (petroleum/ethylacetate (20:1 v/v) as the eluent) to get yellow solid of **4**. Yield 73.3%. Mp: 95 °C $^1\text{H NMR}$: (CDCl_3 , 400 MHz): 9.88 (s, 2H), 7.84 (d, 4H), 7.47 (t, 2H), 7.31 (t, 1H), 7.28 (m, 6H). FT-IR (KBr, cm^{-1}): 1687, 1582, 1502, 1329, 1293, 1213, 1159, 819, 758, 700, 642, 537, 512.

2.3.8. 4,4'-(phenylazanediyldibenzoic acid (**5**)

To a solution of **4** (9.03 g, 30 mmol) in 150 mL of acetone, a solution of KMnO_4 (18.96 g, 120 mmol) and K_2CO_3 (2.75 g, 20 mmol) in 200 mL H_2O was added slowly dropwise. The mixture was refluxed for 7 h, and filtered. The solution was adjusted to pH = 1 with HCl, and then filtered. The crude product was recrystallized from anhydrous ethanol to give 7.32 g yellow crystals



L4

Scheme 3. Synthesis route for **L4**.

Table 1
Crystal data collection and structure refinement of **L1**, **L2** and **L4**.

Compound	L1	L2	L4
Chemical formula	C ₃₂ H ₂₄ N ₄	C ₇₄ H ₅₆ N ₈ O ₈	C ₄₅ H ₃₄ N ₄ O ₄
Formula weight	486.50	1185.27	694.76
Crystal system	Triclinic	Triclinic	Monoclinic
Space group	P1	P1	P2/c
a (Å)	9.298(5)	8.145(5)	16.892(8)
b (Å)	11.366(5)	19.587(5)	19.541(7)
c (Å)	12.783(5)	19.968(5)	11.714(8)
α (°)	107.334(5)	105.366(5)	90
β (°)	98.911(5)	94.884(5)	108.830 (7)
γ (°)	98.521(5)	93.516(5)	90
V (Å ³)	1246.7(10)	3049(2)	3660(3)
Z	2	2	4
R ₁ , wR ₂ [I ≥ 2σ(I)]	0.0428, 0.0980	0.0651, 0.1493	0.0648, 0.1827
R ₁ , wR ₂ (all data)	0.0676, 0.1159	0.1835, 0.2259	0.2081, 0.3324
GOF	0.970	0.916	0.959

5. Yield 73.2%. Mp: 25 °C ¹H NMR: (CDCl₃, 400 MHz): 7.96 (d, 2H), 7.44 (t, 2H), 7.26 (t, 1H), 7.21 (d, 2H), 7.13 (d, 4H). FT-IR (KBr, cm⁻¹): 3425, 3002, 1687, 1593, 1517, 1484, 1419, 1318, 1278, 1173, 848, 765, 704 523.

2.3.9. dimethyl 4,4'-(phenylazanediy) dibenzoate (**6**)

5 (6.66 g, 20 mmol) was dissolved in 200 mL miscible liquids (methanol and H₂SO₄). The mixture was refluxed for 8 h. After the mixture was cooled to room temperature, the most methanol in the mixture was removed. The residue was dispersed into 200 mL of water. The solution was adjusted to pH = 8 with K₂CO₃ and extracted three times with CH₂Cl₂. The solvent was removed in vacuo. The residue was purified by silica gel chromatography column using petroleum/ethylacetate (15:1 v/v) as the eluent. Light yellow solid product **6** was collected. Yield 84.3%. Mp: 80 °C ¹H NMR: (CDCl₃, 400 MHz): 7.93 (d, 4H), 7.36 (m, 2H), 7.28 (s, 1H), 7.17 (m, 7H), 3.91 (s, 6H). FT-IR (KBr, cm⁻¹): 2947, 1715, 1601, 1495, 1427, 1313, 1275, 1098, 853, 751, 691, 527.

2.3.10. dimethyl 4,4'-(4-formylphenylazanediy) dibenzoate (**7**)

6 (3.61 g, 10 mmol) and DMF (5 mL) were mixed cooled in ice bath, and then a solution of POCl₃ (100 mL) was added dropwise for 10 min and refluxed for 7 h. After being cooled to room temperature, the mixture was poured into 200 mL of water and adjusted to

Table 2
Selected bond lengths (Å) and angles (°) for of **L1**, **L2** and **L4**.

L1			
C(4)–N(4)	1.423(2)	C(7)–N(4)	1.430(2)
C(13)–N(4)	1.405(2)	N(2)–N(24)	1.338(2)
N(2)–C(28)	1.331(2)	N(1)–C(22)	1.342(2)
N(1)–C(21)	1.343(2)	N(3)–C(29)	1.333(2)
N(3)–C(32)	1.337(2)	C(4)–N(4)–C(13)	121.00(14)
C(4)–N(4)–C(7)	118.12(13)	C(7)–N(4)–C(13)	120.88(15)
L2			
C(6)–N(1)	1.423(5)	C(9)–N(1)	1.417(5)
C(17)–N(1)	1.442(4)	C(6)–N(1)–C(17)	119.9(3)
C(6)–N(1)–C(9)	121.4(3)	C(9)–N(1)–C(17)	118.7(3)
C(32)–N(3)–C(28)	116.2(4)	C(26)–N(2)–C(24)	117.2(3)
C(33)–N(4)–C(37)	117.3(4)		
L4			
C(21)–C(22)	1.481(8)	C(22)–C(23)	1.224(9)
C(23)–C(24)	1.493(8)	C(29)–N(4)	1.412(6)
C(30)–N(4)	1.430(6)	C(36)–N(4)	1.408(6)
N(1)–C(8)	1.336(5)	N(1)–C(12)	1.338(5)
N(2)–C(7)	1.341(4)	N(2)–C(6)	1.339(4)
N(3)–C(5)	1.328(5)	N(3)–N(1)	1.328(6)
C(20)–C(21)–C(22)	122.9(7)	C(23)–C(22)–C(21)	129.8(9)
C(29)–N(4)–C(30)	118.3(4)	C(29)–N(4)–C(36)	122.9(4)
C(36)–N(4)–C(30)	118.4(4)		

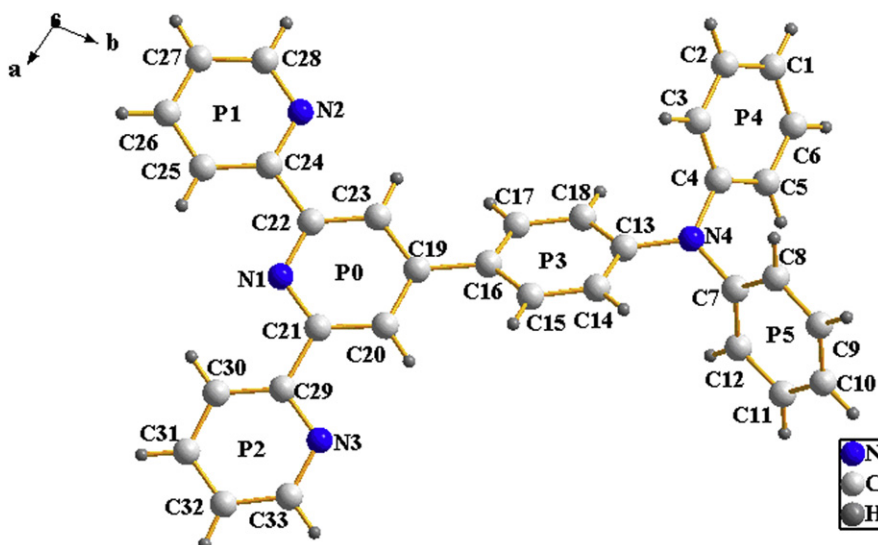
the pH = 1 with sodium hydroxide. The solution was extracted three times with CH₂Cl₂. The organic layer was dried over anhydrous MgSO₄, the residue was purified by silica gel chromatography column using petroleum/ethylacetate (20:1 v/v) as the eluent. Yellow solid product **7** was collected. Yield 78.2%. Mp: 95 °C ¹H NMR (CDCl₃, 400 MHz): 9.92 (s, 1H), 8.01 (m, 4H), 7.80 (m, 2H), 7.13 (m, 6H), 3.93 (s, 6H). Anal. Calcd. for C₂₃H₁₉NO₅: C, 70.98; H, 4.81; N, 10.28; O, 20.62%. Found: C, 70.95; H, 4.88; N, 3.60; O, 20.57%. MS: m/z (%) = 389.13(100). FT-IR (KBr, cm⁻¹): 1723, 1593, 1499, 1322, 1275, 1170, 1173, 830, 769, 700, 527.

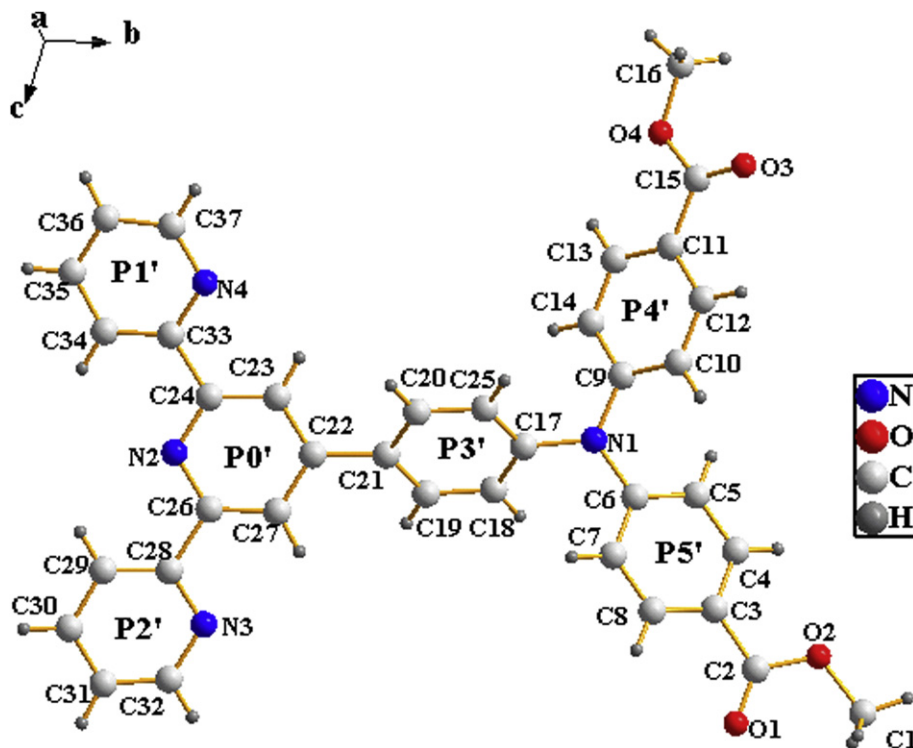
2.3.11. 4-(2,2':6',2''-terpyridyl-4')-benzyl triphenyl phosphonium bromide (**9**)

9 was synthesized according to literature method [35,36].

2.3.12. 4'-(4-[2-[dimethyl 4,4'-(phenylazanediy) dibenzoate] ethenyl]phenyl)-2,2':6',2''-terpyridine (**L4**)

t-BuOK (1.20 g, 10 mmol) was placed into a dry mortar, then **9** (3.40 g, 5 mmol) and **7** (1.00 g, 2.6 mmol) were mixed, and milled

Fig. 1. Crystal structure of **L1**.

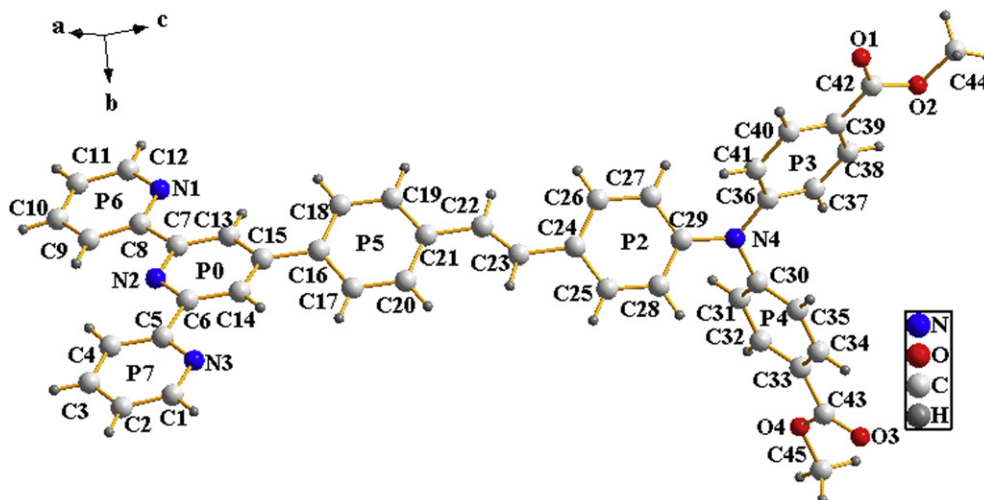
Fig. 2. Crystal structure of **L2**.

vigorously for about 30 min. After completion of the reaction (monitored by TLC), the mixture was dispersed in 200 mL of dichloromethane, the solvent was removed in vacuo, filtered and the solution was extracted with CH_2Cl_2 . The residue was purified by silica gel chromatography column using petroleum/ethylacetate (10:1 v/v) as the eluent. Solid product **L4** was collected. Yield 70.2%. ^1H NMR (CDCl_3 , 400 MHz): 8.83 (t, 6H), 8.18 (m, 2H), 8.03 (d, 2H), 7.87 (m, 6H), 7.70 (m, 4H), 7.45–7.41 (d, $J = 16.00$, 1H), 7.37–7.33 (d, $J = 16.00$, 1H), 7.15 (m, 6H), 3.83 (s, 6H). ^{13}C NMR (CDCl_3 , 100 MHz): 166.6, 156.2, 155.9, 150.8, 149.6, 149.1, 145.5, 138.1, 137.4, 136.9, 134.1, 131.1, 128.4, 127.9, 127.6, 127.0, 126.2, 124.4, 123.8, 122.7, 121.4, 118.5, 52.0. Anal. Calcd. for $\text{C}_{45}\text{H}_{34}\text{N}_4\text{O}_4$: C, 77.78; H, 4.88; N, 7.91; O, 9.25%. Found: C, 77.81; H, 4.90; N, 8.07; O, 9.22%. MS: m/z (%) = 694.25 (100). FT-IR (KBr, cm^{-1}):

3444, 3036, 2924, 2854, 1717, 1641, 1596, 1544, 1509, 1489, 1463, 1435, 1395, 1318, 1274, 1177, 1110, 1075, 1031, 994, 968, 911, 832, 791, 756, 739, 695, 610, 531.

3. Results and discussion

The synthesis of the ligands (**L2** and **L4**) was illustrated in Scheme 2 and 3. **L1** and **L3** were synthesized according to literature method [34,35]. And through the Solvent-free Wittig or Friedel–Crafts reactions, **L2** and **L4** were synthesized in high yields, and purified either using recrystallization or column chromatography. The structures of ligands were confirmed by IR, ^1H NMR, and ^{13}C NMR spectra. Mass spectra and elemental analyses were used to further verify the structures of the chromophores. Additionally,

Fig. 3. Crystal structure of **L4**.

their crystal structures were determined by single crystal X-ray diffraction analysis.

3.1. Crystal structures of **L1**, **L2** and **L4**

The crystal data collection, and refinement parameters are listed in Table 1. Selected bond lengths and angles are given in Table 2.

The crystal structures of **L1** and **L2** are shown in Fig. 1 and Fig. 2, respectively. As shown in Fig. 1, chromophore **L1** consists of terpyridyl (acceptor) and triphenylamine (donor) moieties. The central pyridinyl (labeled P0) is arranged with a phenyl (P3) and two pyridine planes (P1 and P2) being 4.16° (P0 and P1), 6.79° (P0 and P2) and 32.50° (P0 and P3). The result indicates that the terpyridyl group is seldom coplanar. At the diphenylamino donor end, the central nitrogen and its three bended carbon atoms are basically coplanar, forming a quasi-equilateral trigonal NC3 plane (defined as the P6 plane), with the sum of the three C–N–C angles (360.0°). Around the central nitrogen, three phenyl ring planes (P3, P4 and P5, respectively) are arranged in a propeller-like fashion (P3 and P6: 29.47°, P4 and P6: 49.36°, P5 and P6: 64.82°).

Compared with **L1**, it is difference that the crystal structure of **L2** is shown in Fig. 2, methylformate groups attached to the triphenylamine moiety in the molecule **L2** make the whole molecular structure changes: (1) In the terpyridyl acceptor moiety, the central pyridinyl (labeled P0') is arranged with a phenyl (P3') and two pyridine planes (P1' and P2') being 9.18° (between P0' and P1'), 8.83° (P0' and P2') and 37.00° (P0' and P3'); (2) Around the central nitrogen N1, three phenyl ring planes (P3', P4' and P5', respectively) are differently arranged in a propeller-like fashion with angles: P3' and P6: 45.87°, P4' and P6: 35.04°, P5' and P6: 30.97°.

The crystal structure of **L4** is shown in Fig. 3. Compared with the crystal structure of **L3** [35], methylformate groups attached to the triphenylamine moiety make molecular structure changes: the parameters are presented in Table 3. The linkage between two phenyl rings (P2 and P5) is quite conjugated with bond lengths C(21)–C(22): 1.481(8) Å, C(22)=C(23): 1.224(9) Å and C(23)–C(24): 1.493(8) Å. It can be seen from Table 2 that all the bond lengths of C–C are located between the normal C=C double bond (1.34 Å) and C–C single bond (1.54 Å), which show that there is a higher delocalized π -electron system in **L4** molecule. Because crystallographic disorder appears in C(22) and C(23), the bond length of C(22)–C(23) (1.224(9) Å) is shorter than the normal C=C bond length.

To summarize, the donor-acceptor (D-A) (**L1** and **L2**) and donor- π -acceptor (D- π -A) types (**L3** and **L4**) from 2, 2': 6', 2''-terpyridine-based organic heterocyclic molecules were crystallographically confirmed. Methylformate groups attached to the triphenylamine moiety make the conformation of the molecular structures, bond angles and bond lengths changes. The structural features suggest that all nonhydrogen atoms are highly conjugated, leading to the charge transfer from triphenylamine and ethylformate groups to terpyridyl moiety.

Table 3
Conformational parameters for **L3** and **L4**.

	L3	L4
P _{0,5}	14.1°	27.07°
P _{0,6}	7.0°	7.98°
P _{0,7}	2.3°	5.70°
P _{1,2}	43.2°	42.06°
P _{1,3}	34.4°	24.86°
P _{1,4}	43.7°	55.79°

P_{0,5} represent the dihedral angles between P0 and P5, and so on.

Table 4
Single-photon-related photophysical properties of **L1**, **L2**, **L3** and **L4** in several different solvents.

Cmpd	Solvents	λ_{\max}^a (ϵ_{\max}^b)	λ_{\max}^c	Φ^d	τ/ns^e
L1	C ₆ H ₆	289(4.47) 359(3.41)	430	0.56	2.37
	CH ₂ Cl ₂	287(4.54) 357(3.43)	465	0.52	3.97
	THF	286(4.94) 355(3.81)	449	0.63	3.43
	CH ₃ COOC ₂ H ₅	286(4.68) 354(3.71)	454	0.54	3.27
	CH ₃ CN	283(4.67) 353(3.66)	492	0.22	4.89
	DMF	286(5.07) 357(3.73)	487	0.40	5.25
L2	C ₆ H ₆	276(4.18) 353(6.77)	404	0.45	1.45
	CH ₂ Cl ₂	278(3.52) 352(6.94)	427	0.38	1.77
	THF	276(3.67) 349(6.75)	421	0.41	1.55
	CH ₃ COOC ₂ H ₅	276(3.43) 348(6.53)	417	0.42	1.56
	CH ₃ CN	277(3.47) 349(6.32)	450	0.41	2.61
	DMF	277(3.38) 352(5.97)	446	0.48	2.52
L3	C ₆ H ₆	296(4.55) 386(3.98)	461	0.32	1.38
	CH ₂ Cl ₂	294(4.82) 386(4.19)	510	0.23	2.09
	THF	294(4.65) 383(4.22)	494	0.34	1.88
	CH ₃ COOC ₂ H ₅	292(5.01) 381(4.23)	494	0.36	1.79
	CH ₃ CN	290(4.96) 381(4.24)	526	0.19	2.61
	DMF	294(4.61) 387(4.74)	526	0.17	2.60
L4	C ₆ H ₆	286(4.37) 360(6.01)	440	0.41	1.08
	CH ₂ Cl ₂	279(5.52) 356(6.29)	426, 443	0.26	1.54
	THF	289(4.49) 356(6.61)	468	0.38	1.44
	CH ₃ COOC ₂ H ₅	285(4.70) 355(6.52)	463	0.39	1.38
	CH ₃ CN	287(4.50) 355(6.76)	506	0.25	1.95
	DMF	290(4.49) 360(6.72)	505	0.29	1.95

^a Peak position of the longest absorption band.

^b Maximum molar absorbance in 10⁴ mol⁻¹ L cm⁻¹.

^c Peak position of SPEF, exited at the absorption maximum.

^d Quantum yields determined by using RhB and coumarin as standard.

^e The fitted fluorescence lifetime.

3.2. Absorption and single-photon excited fluorescence (SPEF)

3.2.1. Linear absorption properties and TD-DFT studies

The photophysical data of the compounds were summarized in Table 4. The linear absorption, emission and two-photon absorption spectra of **L1** and **L2** in six organic solvents are shown in Fig. 4 (Fig. S1), from which one can see that their absorption spectra exhibit dual bands in the 270–400 nm range in all the solvents. The low-energy band was tentatively assigned to the $\pi \rightarrow \pi^*$ or intraligand charge transfer (ICT) transition, while the high-energy band was assigned to the $\pi \rightarrow \pi^*$ transition of the triphenylamine moiety. As shown in Fig. S1 and Table 4, weak solvatochromism was

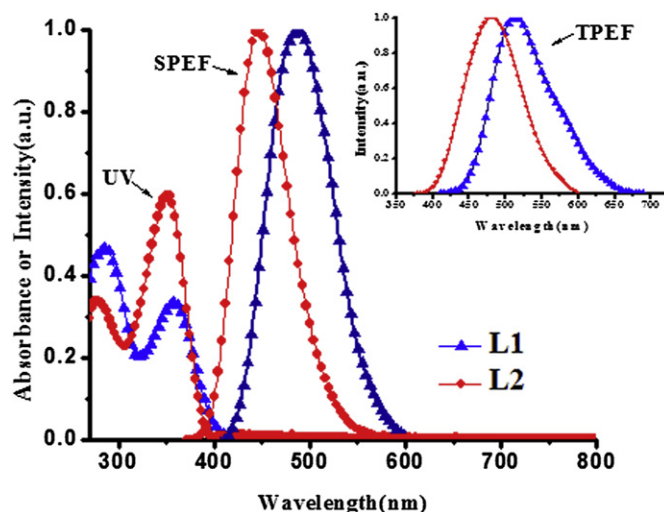


Fig. 4. Linear absorption ($c = 1 \times 10^{-5}$ mol L⁻¹), SPEF ($c = 1 \times 10^{-5}$ mol L⁻¹) and TPEF ($c = 1 \times 10^{-3}$ mol L⁻¹) spectra of **L1** and **L2** in DMF, respectively.

observed, indicating the **L1–4** molecules with fairly small dipole moments and the difference in dipoles between ground and excited state [37]. It was also found that the methylformate, as a peripheral substituting groups attached to the triphenylamine moiety, make the absorption bands blue-shifted and the intensity of the high-energy band decrease for the compounds (**L2**, **L4**). The results will be further corroborated by calculations.

TD-DFT computational studies were performed to elucidate the electronic structures of the ground state of **L1–4**. The schematic representation of the molecular orbitals of **L1–4** was exhibited in Figs. 5 and 6, Figs. S2 and S3, and the energies and compositions of some frontier orbitals are listed in Table 5. The absorption spectra of the investigated chromophores show similar features, while transitions of the main $\pi \rightarrow \pi^*$ character were found at a higher energy.

Fig. 5 shows the calculated frontier orbitals of (**L1**). The band calculated is at 330 nm, which mainly originates from transitions of HOMO–1 to LUMO. At shorter wavelengths, a broad band found at 285 nm around may be related to the calculated intense band at 281 nm, corresponding to the HOMO–1 to LUMO+2. Fig. 6 shows the calculated frontier orbitals of (**L2**). The lowest energy band calculated is at 359 nm. This band mainly originates from transitions of HOMO to LUMO+2, which can be assigned to a charge transfer (CT) transition due to the triphenylamine characteristic HOMO and terpyridyl with triphenylamine characteristic LUMO. At shorter wavelengths, a band found at 275 nm approximately may be related to the calculated intense band at 280 nm. The transition corresponds to the HOMO–1 to LUMO+1. The experiment and theoretical calculation are consistent. Overall, these initial DFT and

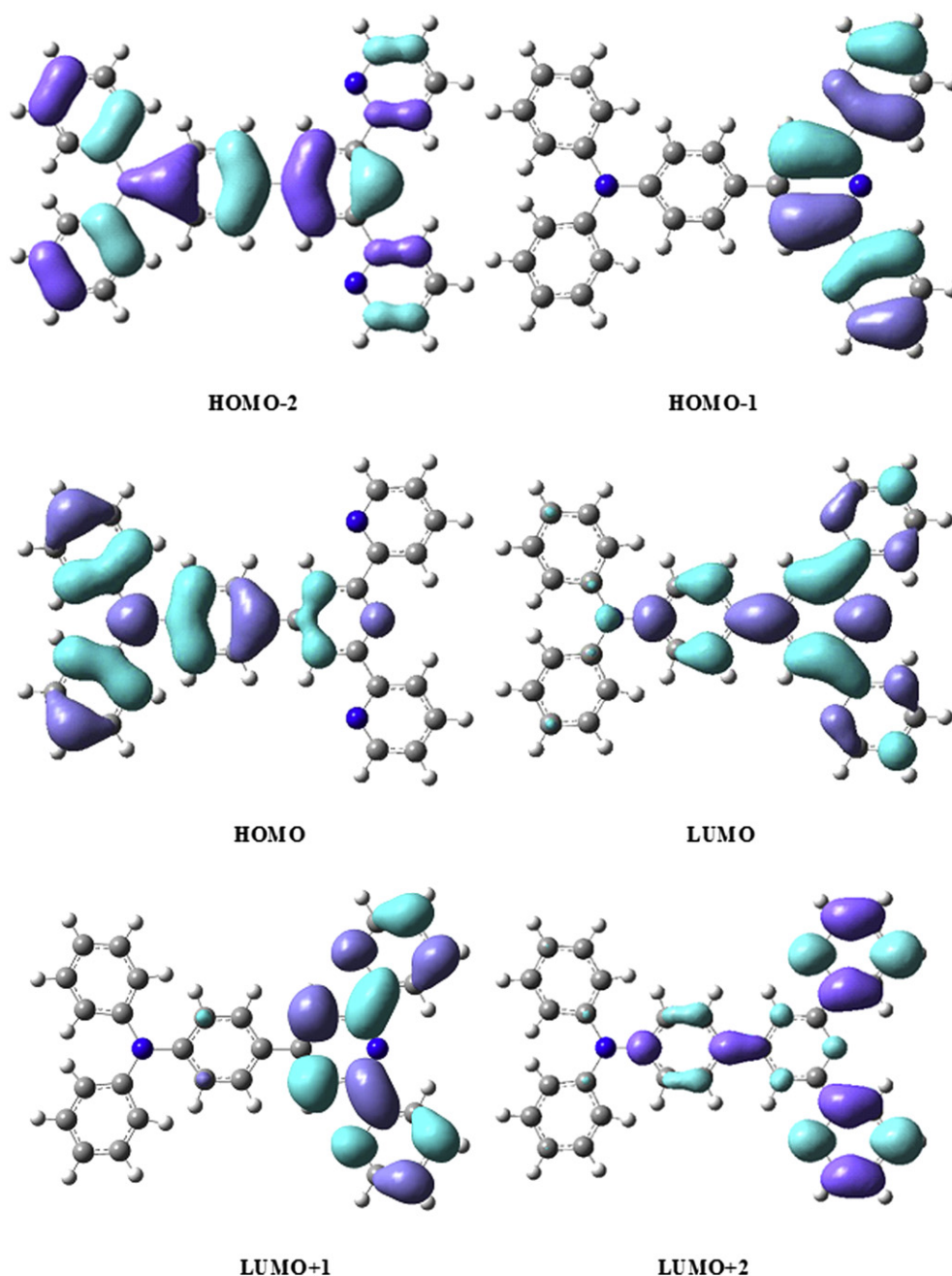


Fig. 5. Molecular orbital energy diagram for **L1** (DFT/B3LYP).

TD-DFT calculations on (**L1**, **L2**, **L3** and **L4**) provide reasonable explanations for their absorption spectra.

3.2.2. Single-photon excited fluorescence (SPEF)

The one-photon fluorescence spectra of the series of chromophores in six different solvents are collected in Table 4, including fluorescence quantum yields and lifetimes (corresponding figures are given in Supporting information). Their emission range can be tuned by changing the nature of the peripheral substituting groups and of the polarity of the solvents. In addition, all the chromophores exhibit high fluorescence quantum yields in the different solvents. With increasing polarity of the solvent, their single-photon excited fluorescence (SPEF) spectra show remarkable bathochromic shifts. As shown in Fig. 7, for example, λ_{\max} (SPEF) of **L1** is located at 430 nm in toluene and red-shifted to 492 nm in acetonitrile, indicating that this charge separation increases in the excited state, resulting in a larger dipole moment than that in the ground state, which explain the sensitivity of the emission spectra of these dipolar compounds to solvent polarity [38]. Besides, as shown in Fig. S4, the two peaks phenomenon in the minimum polar solvent of benzene and CH_2Cl_2 , has been observed for the fluorescence intensity of **L4**, which may be attributed to the twisted intramolecular charge transfer (TICT) [39]. Furthermore, with increasing polarity of the solvent, as shown in Fig. 8 (Fig. S5), fluorescence lifetime of the chromophores also increased. These results suggest that the molecular polarity of the fluorescent excited state must be larger than that of the ground state, as the enhanced dipole–dipole interactions caused by increasing the polarity of the solute and/or solvent will lead to a more significant energy level decrease for the excited state. Compared with those of **L1** and **L3**, fluorescence lifetime of **L2** and **L4** decreased, although

their same principle part framework, due to the methylformate group attached to the triphenylamine moiety.

3.3. Two-photon excited fluorescence (TPEF)

Detailed experiments reveal that there is no linear absorption in the wavelength range 500–900 nm for all the chromophores, which indicates that there are no molecular energy levels corresponding to an electron transition in the spectral range. Therefore, upon excitation from 500 to 910 nm, it is impossible to produce single-photon-excited up-converted fluorescence. The linear dependence on the square of input laser power suggests a two-photon excitation mechanism at 720 nm for the chromophores Fig. 9 (Fig. S6).

As shown in Fig. 10 (Fig. S7), for example, upon excitation at the optimal wavelengths, the TPEF spectra of **L2** in different solvents are presented. It exhibits positive solvatochromism effect, the same trend as the one photon fluorescence. One can see that **L1**, **L2**, **L3** and **L4** exhibit two-photon fluorescence and the TPEF peak positions show a red-shift. This can be explained by the effect of reabsorption. We can clearly observe the strongest intensity of the TPEF in high polar solvent DMF, while according to most of the literature reports, the action has taken place usually in the nonpolar solvent.

As shown in Fig. S8, two-photon absorption cross sections (δ) of **L1**, **L2**, **L3** and **L4** have been measured using two-photon-induced fluorescence measurement technique described in the experiments. The maximum two photon absorption cross sections are 434 GM for **L1**, 179 GM for **L2**, 2869 GM for **L3** and 1019 GM for **L4** in DMF, which is basically the same with theoretical calculation result trend (Table 6). Fig. 11 shows the TPA action spectra of **L1**, **L2**, **L3** and

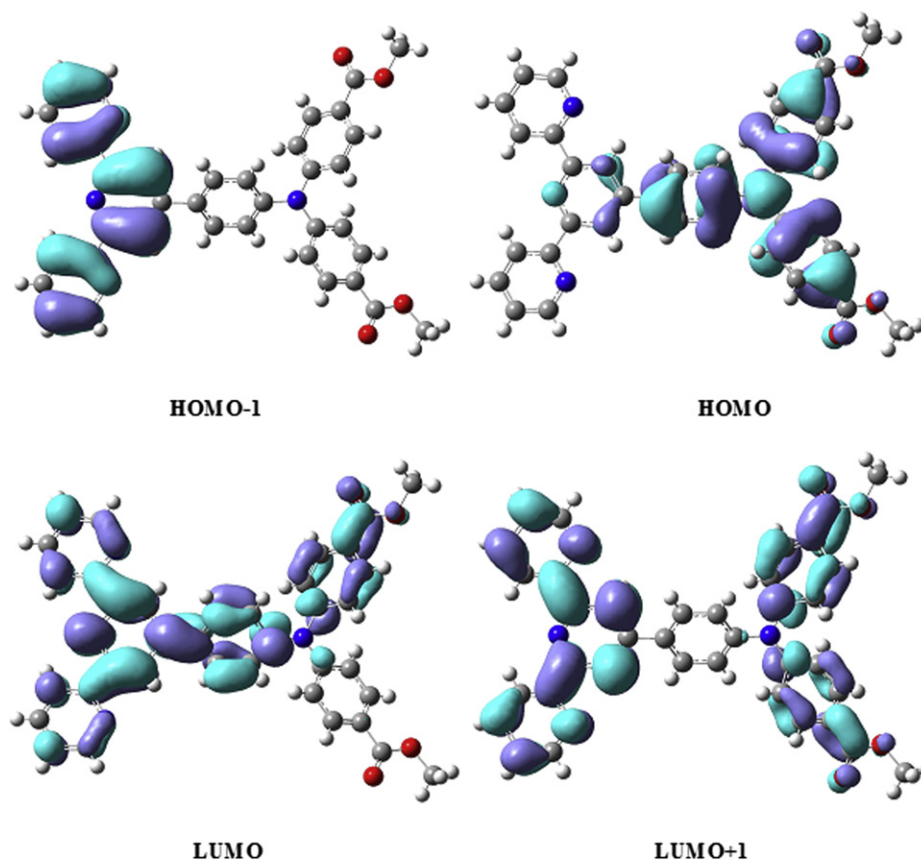


Fig. 6. Molecular orbital energy diagram for **L2** (DFT/B3LYP).

Table 5
Calculated linear absorption properties (nm), excitation energy (ev), oscillator strengths and major contribution for **L1**, **L2**, **L3** and **L4**.

Cmpd	λ (nm)	E (ev)	f	Composition
L1	330.19	3.75	0.1778	124 → 126 (H-1 → L) (0.62819)
	281.68	4.40	0.2084	124 → 128 (H-1 → L + 2) (0.44483)
L2	359.33	3.45	0.4485	155 → 158 (H → L + 2) (0.52632)
	280.10	4.42	0.1738	155 → 158 (H-1 → L + 1) (0.50160)
L3	379.65	3.26	0.2773	152 → 154(H → L + 2) (0.67296)
	288.54	4.29	0.1548	150 → 155 (H-2 → L + 2) (0.65977)
L4	343.58	3.61	0.1785	181 → 183 (H-1 → L) (0.46787)
	295.54	4.19	0.1099	180 → 186 (H-2 → L + 3) (0.48421)

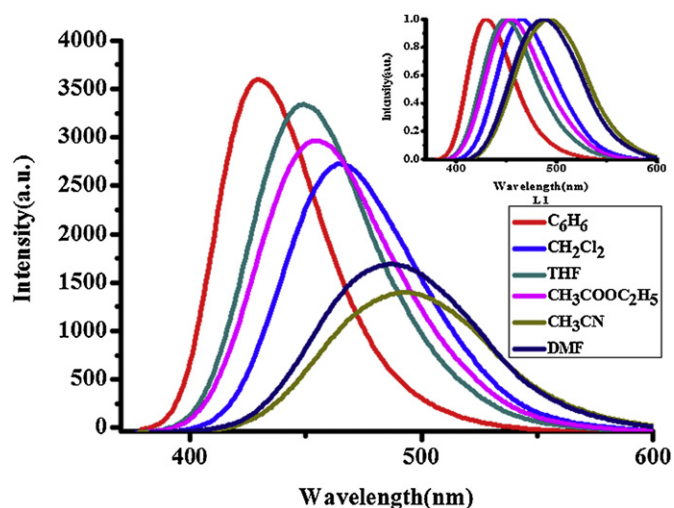


Fig. 7. One-photon fluorescence spectra of **L1** in six solvents with a concentration of 1×10^{-5} mol L⁻¹, respectively.

L4 in the 680–910 nm range in DMF. It has been found that two-photon absorption cross sections of **L3** and **L4** in the wavelength range (680–910 nm) are larger than that of **L1** and **L2**. The behavior, observed here in the TPA cross sections, can be attributed to the enlarged conjugation of **L3** and **L4** compared to **L1** and **L2**, a new D- π -A type chromophore, in which the terpyridyl ring is the acceptor part and triphenylamine is the donor one. At the same time, the δ values of **L4** compared to those of **L3**, and the δ values of **L2** compared to those of **L1** in the wavelength range (from 680

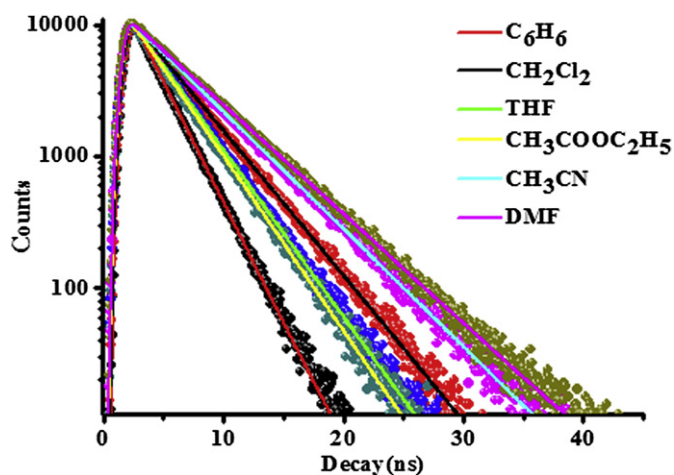


Fig. 8. Time-resolved fluorescence curves of **L1** in six solvents.

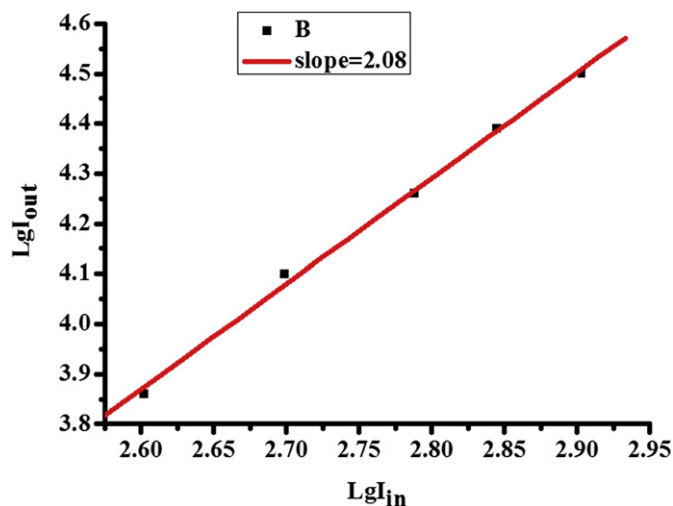


Fig. 9. Output fluorescence (I_{out}) vs. the square of input laser power (I_{in}) for **L2** excitation carried out at 720 nm, with $c = 1.0 \times 10^{-3}$ mol L⁻¹ in DMF.

to 910 nm) are always smaller, which can be attributed to the methylformate groups as a peripheral substituting units attached to the triphenylamine moiety.

4. Theoretical calculation

The two-photon absorption cross-section that can be directly compared with the experimental results is defined as:

$$\sigma_{tp} = \frac{4\pi^2 a_0^5 \alpha}{15c_0} \times \frac{\omega^2 g(\omega) \delta_{tp}}{\Gamma_f} \quad (1)$$

Here a_0 is the Bohr radius, c_0 is the speed of light, α is the fine structure constant, ω is the photon frequency of the incident light, and $g(\omega)$ denotes the spectral line profile, which is assumed to be a δ function here, Γ_f is the lifetime broadening of the final state, which is commonly assumed to be 0.1 eV [40], and σ_{tp} is orientation average value of the two-photon absorption probability in gas and solution, which is written as follows [41],

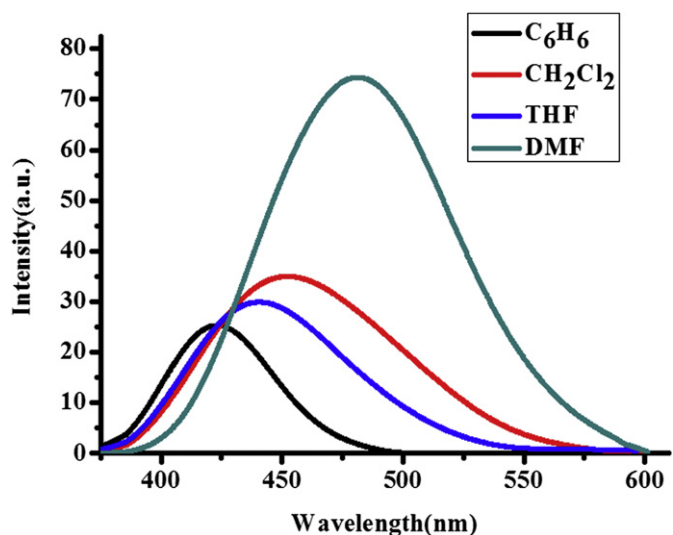


Fig. 10. The two-photon fluorescence spectra of **L2** in different solvents with the same concentration of 1.0×10^{-3} mol L⁻¹ in $\lambda_{em} = 720$ nm.

Table 6

The two-photon absorption cross-section δ_{tp} (1 GM = 10^{-50} cm⁴ s/photon) of the six lowest excited states with the excitation energy E (eV) and the corresponding wavelength λ_{tp} (nm) in the gas phase.

E	λ_{tp}	δ_{tp}	E	λ_{tp}	δ_{tp}
L1			L2		
3.39	729.53	262.77	3.48	710.66	177.51
3.40	727.38	0.04	3.63	681.30	16.90
4.01	616.73	0.19	3.65	677.56	33.19
4.14	597.37	18.33	4.10	603.20	5.49
4.19	590.24	23.54	4.11	601.73	290.93
4.28	577.83	0.00	4.23	584.66	0.03
L3			L4		
3.11	795.21	857.71	3.22	768.04	486.32
3.41	725.25	0.04	3.58	690.81	82.56
3.67	673.87	284.29	3.69	670.22	0.00
3.94	627.69	0.75	3.84	644.04	836.45
4.05	610.64	542.15	4.00	618.28	637.90
4.10	603.20	0.49	4.05	610.64	3.43

$$\delta_{tp} = \sum_{\alpha\beta} \left[F \times S_{\alpha\alpha} \times S_{\beta\beta}^* + G \times S_{\alpha\beta} \times S_{\alpha\beta}^* + H \times S_{\alpha\beta} \times S_{\beta\alpha}^* \right] \quad (2)$$

Where F , G , and H are coefficients dependent on the polarization of the light. For the linearly polarized light, F , G and H are 2,2,2, for the circularly case, they are $-2,3,3$. $S_{\alpha\beta}$ is the two-photon transition matrix element. For the absorption of two photons with the same frequency $\omega_f/2$ it can be written as [42],

$$S_{\alpha\beta} = \sum_i \left[\frac{\langle 0|\mu_\alpha|i\rangle\langle i|\mu_\beta|f\rangle}{\omega_i - \omega_f/2} + \frac{\langle 0|\mu_\beta|i\rangle\langle i|\mu_\alpha|f\rangle}{\omega_i - \omega_f/2} \right] \quad (3)$$

Where ω_i and ω_f denote the excitation frequency of the intermediate state $|i\rangle$ and final state $|f\rangle$ respectively, $\alpha, \beta \in (x, y, z)$, and the summation goes over all the intermediate states including the ground state $|0\rangle$ and the final state $|f\rangle$.

We use the GUASSIAN package [43] to optimize the molecule geometries in gas phase at the HF/6-31G* level. The calculation two-photon absorption is carried out by the response theory method [44] at the DFT level implemented in DALTON program [45].

The nonlinear optical properties of **L1**, **L2**, **L3** and **L4** in gas phase are listed in Table 5, from which we can observe that the calculated

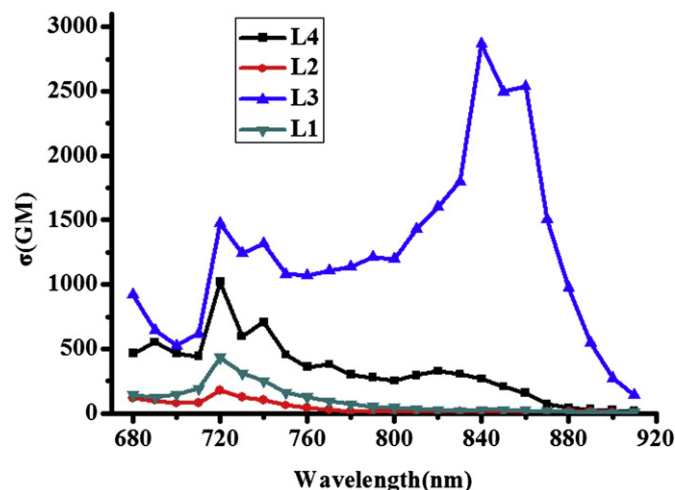


Fig. 11. Two-photon (from a 140 fs, 76 MHz Ti:sapphire laser) absorption cross sections of **L1**, **L2**, **L3** and **L4** in DMF vs. excitation wavelengths of identical energy of 0.500 W.

optical properties depend on the different geometries. The largest two-photon absorption cross-section of the molecules is 486.32 for **L4**, 857.71 for **L3**, 177.51 for **L2**, and 262.77 GM for **L1** (1 GM = 10^{-50} cm⁴s/photon). Theoretical calculation is consistent with the experimental result trend (**L3** > **L4** > **L1** > **L2**) described above.

5. Conclusions

Four terpyridine-based chromophores with large two-photon absorption cross sections were obtained. One-photon absorption and emission spectra, two-photon excited fluorescence action have been systematically investigated. The relationships between the structures and photophysical properties for the series compounds can be understood based on both the experimental and theoretical results. It was found that both **L2** and **L4** possess smaller δ_{max} than those of **L1** and **L3**, due to the methylformate terminal groups attached to the triphenylamine moiety leading to a decreased amount of pushing-electron ability in the molecular **L2** and **L4**, as well as make the whole molecular structure and properties changes. It is noteworthy that the four chromophores have the strongest TPEF intensity in high polar solvent, such as DMF, which has potential applications in biology. Importantly, the two kinds of chromophores (**L2** and **L4**) can coordinate with metal ions after methylformate terminal groups hydrolysis, which has potential applications in metal ion sensors and fluorescence probe.

Acknowledgments

This work was supported by a grant for the National Natural Science Foundation of China (21071001, 51142011 and 21101001), Department of Education of Anhui Province (KJ2010A030), Foundation of the Scientific Innovation Team of Anhui Province (2006KJ007TD), The 211 Project of Anhui University, Ministry of Education Funded Projects Focus on returned overseas scholar. The Foundation for Outstanding Youth of the Department of Science and Technology of Anhui Province (10040606Y22).

Appendix A. Supplementary data

Supplementary data associated with this article can be found, in the online version, at doi:10.1016/j.dyepig.2012.03.020.

References

- [1] Wampler RD, Moad AJ, Moad CW, Heiland R, Simpson GJ. Visual methods for interpreting optical nonlinearity at the molecular level. *Acc Chem Res* 2007; 40:953–60.
- [2] Chemla D, Zyss J. *Nonlinear optical properties of organic molecules and crystals*, vol. 1. New York: Academic Press; 1987. 23–187.
- [3] Poornesh P, Seetharam S, Umesh G, Manjunatha KB, Kamath KP, Sarojini BK, et al. Nonlinear optical studies on 1,3-disubstituted chalcones doped polymer films. *Opt Mater* 2009;31:854–9.
- [4] Lin TC, Huang YJ, Chen YF, Hu CL. Two-photon absorption and effective broadband optical power limiting properties of a multi-branched chromophore containing 2,3-diarylquinoxalanyl moieties as the electron-pulling units. *Tetrahedron* 2010;66:1375–82.
- [5] Lemerrier G, Mulateur JC, Martineau C, Anémian R, Andraud C, Wang IO, et al. Two-photon absorption: from optical power limiting to 3D microfabrication. *C R Chim* 2005;8:1308–16.
- [6] Wang XS, Qiu JR, Song J, Xu J, Liao Y, Sun HY, et al. Upconversion luminescence and optical power limiting effect based on two- and three-photon absorption processes of ZnO crystal. *Opt Commun* 2007;280:197–201.
- [7] Milan B, Hazel AC, Emma D, Harry LA. Synthesis of hydrophilic conjugated porphyrin dimers for one-photon and two-photon photodynamic therapy at NIR wavelengths. *Org Biomol Chem* 2009;7:874–88.
- [8] Zhu MQ, Zhang GF, Li C, Matthew PA, Emmanuel C, Rebekah AD, et al. Reversible two-photon photoswitching and two-photon imaging of immunofunctionalized nanoparticles targeted to cancer cells. *J Am Chem Soc* 2011; 133:365–72.

- [9] Xiao HB, Li H, Chen MJ, Wang L. A water-soluble D- π -A chromophore based on dipicolinic acid: synthesis, pH-dependent spectral properties and two-photon fluorescence cell imaging. *Dyes Pigm* 2009;83:334–8.
- [10] (a) Dong XH, Yang YY, Sun J, Liu ZH, Liu BF. Two-photon excited fluorescent probes for calcium based on internal charge transfer. *Chem Commun*; 2009:3883–5; (b) Hai Y, Chen JJ, Zhao P, Lv HB, Yu Y, Xu PY, et al. Luminescent zinc salen complexes as single and two-photon fluorescence subcellular imaging probes. *Chem Commun* 2011;47:2435–7.
- [11] Zheng QD, He GS, Paras NP. A novel near IR two-photon absorbing chromophore: optical limiting and stabilization performances at an optical communication wavelength. *Chem Phys Lett* 2009;475:250–5.
- [12] Kazuya O, Yoshiaki K. Design of two-photon absorbing materials for molecular optical memory and photodynamic therapy. *Org Biomol Chem* 2009;7:2241–6.
- [13] Belfield KD, Liu Y, Negres RA, Fan M, Pan G, Hagan DJ, et al. Two-photon photochromism of an organic material for holographic recording. *Chem Mater* 2002;14:3663–7.
- [14] Michael S, Michael F, Zeng CY, Valerică R. Real-time monitoring of two-photon photopolymerization for use in fabrication of microfluidic devices. *Lab Chip* 2009;9:819–27.
- [15] Lee KS, Kim RH, Yang DY, Park SH. Advances in 3D nano/microfabrication using two-photon initiated polymerization. *Prog Polym Sci* 2008;33:631–81.
- [16] Zhou WH, Kuebler SM, Braun KL, Yu TY, Cammack JK, Ober CK, et al. An efficient two-photon-generated photoacid applied to positive-tone 3D microfabrication. *Science* 2002;296:1106–9.
- [17] Park SH, Yang DY, Lee KS. Two-photon stereolithography for realizing ultraprecise three-dimensional nano/microdevices. *Laser Photon Rev* 2009;3:1–2.
- [18] Jiang YH, Wang YC, Wang B, Yang JB, He NN, Qian SX, et al. Synthesis, two-photon absorption and optical limiting properties of multibranched styryl derivatives based on 1,3,5-triazine. *Chem Eur J* 2011;17:2479–91.
- [19] Ji ZQ, Li YJ, Pritchett TM, Makarov NS, Haley JE, Li ZJ, et al. One-photon photophysics and two-photon absorption of 4-[9,9-di-(2-ethylhexyl)-7-diphenylamino-fluoren-2-yl]-2,2':6',2''-terpyridine and their platinum chloride complexes. *Chem Eur J* 2011;17:279–2491.
- [20] Wang Bing, Wang YC, Hua JL, Jiang YH, Huang JH, Qian SX, et al. Starburst triarylamine donor-acceptor-donor quadrupolar derivatives base-on cyano-substituted diphenylaminestyrylbenzene: tunable aggregation-induced emission colors and large two-photon absorption cross sections. *Chem Eur J* 2011;17:2647–55.
- [21] Wild A, Winter A, Schlütter F, Schubert US. Advances in the field of π -conjugated 2,2':6',2''-terpyridines. *Chem Soc Rev* 2011;40:1459–511.
- [22] Constable EC. 2,2':6',2''-Terpyridines: from chemical obscurity to common supramolecular motifs. *Chem Soc Rev* 2007;36:246–53.
- [23] Cummings SD. Platinum complexes of terpyridine: interaction and reactivity with biomolecules. *Coord Chem Rev* 2009;253:1495–516.
- [24] Ghosh S, Chaitanya GK, Bhanuprakash K, Nazeeruddin MK, Grätzel M, Reddy PY. Electronic structures and absorption spectra of linkage isomers of trithiocyanato(4,4',4''-tricarboxy-2,2':6,2''-terpyridine)ruthenium(II) complexes: a DFT study. *Inorg Chem* 2006;45:7600–11.
- [25] Eryazici I, Moorefield CN, Newkome GR. Square-planar Pd(II), Pt(II), and Au(III) terpyridine complexes: their syntheses, physical properties, supramolecular constructs, and biomedical activities. *Chem Rev* 2008;108:1834–95.
- [26] Hayami S, Komatsu Y, Shimizu T, Kamihata H, Lee YH. Spin-crossover in cobalt(II) compounds containing terpyridine and its derivatives. *Coord Chem Rev* 2011;255:1981–90.
- [27] Tian YP, Li L, Zhang JZ, Yang JX, Zhou HP, Wu JY, et al. Investigations and facile synthesis of a series of novel multi-functional two-photon absorption materials. *J Org Chem* 2007;17:3646–54.
- [28] Wang G, Pu KY, Zhang XH, Li K, Wang L, Cai LP, et al. Star-shaped glycosylated conjugated oligomer for two-photon fluorescence imaging of live cells. *Chem Mater* 2011;23:4428–34.
- [29] (a) Hrobárik P, Hrobáriková V, Sigmundová I, Zahradník Pavol, Fakis M, Polyzos I, et al. Benzothiazoles with tunable electron-withdrawing strength and reverse polarity: a route to triphenylamine-based chromophores with enhanced two-photon absorption. *J Org Chem* 2011;76:8726–36; (b) Jiang YH, Wang YH, Hua JL, Tang J, Li B, Qian SX, et al. Multibranching triarylamine end-capped triazines with aggregation-induced emission and large two-photon absorption cross-sections. *Chem Commun* 2010;46:4689–91.
- [30] Demas JN, Crosby GA. Measurement of photoluminescence quantum yields. *J Phys Chem* 1971;75:991–1024.
- [31] Gray TG, Rudzinski CM, Meyer EE, Holm RH, Nocera DG. Spectroscopic and photophysical properties of hexanuclear rhenium(III) chalcogenide clusters. *J Am Chem Soc* 2003;125:4755–70.
- [32] Xu C, Webb WW. Measurement of two-photon excitation cross sections of molecular fluorophores with data from 690 to 1050 nm. *J Opt Soc Am B* 1997;13:481–91.
- [33] Varnavski O, Goodson T, Sukhomlinova L, Twieg R. Ultrafast exciton dynamics in a branched molecule investigated by time-resolved fluorescence, transient absorption, and three-pulse photon echo peak shift measurements. *J Phys Chem B* 2004;108:10484–92.
- [34] Qiu DF, Zhao Q, Bao XY, Liu KC, Wang HW, Guo YC, et al. Electropolymerization and characterization of an alternatively conjugated donor-acceptor metallopolymer: poly-[Ru(4'-(4-(diphenylamino) phenyl)-2,2':6',2''-terpyridine)]²⁺. *Inorg Chem Commun* 2011;14:296–9.
- [35] Hu ZJ, Yang JX, Tian YP, Zhou HP, Tao XT, Bao G, et al. Synthesis and optical properties of two 2,2':6',2''-terpyridyl-based two-photon initiators. *J Mol Struct* 2007;839:50–7.
- [36] Hu ZJ, Yang JX, Tian YP, Tao XT, Tian L, Zhou HP, et al. Synthesis, structures, and optical properties of two novel two-photon initiators derived from 2,2':6',2''-terpyridine. *Bull Chem Soc Jpn* 2007;80:86–993.
- [37] (a) Grabowski ZR, Krystyna R. Structural changes accompanying intramolecular electron transfer: focus on twisted intramolecular charge-transfer states and structures. *Chem Rev* 2007;103:3899–4032; (b) Woo HY, Liu B, Kohler B, Korystov D, Mikhailovsky A, Bazan GC. Solvent effects on the two-photon absorption of distyrylbenzene chromophores. *J Am Chem Soc* 2005;127:14721–9.
- [38] Zhou HP, Zhou FX, Wu P, Zheng Z, Yu ZP, Chen YX, et al. Three new five-coordinated mercury (II) dyes: structure and enhanced two-photon absorption. *Dyes Pigm* 2011;91:237–47.
- [39] Drobizhev M, Karotki A, Dzenis Y, Rebane A, Suo Z, Spangler CW. Strong cooperative enhancement of two-photon absorption in dendrimers. *J Phys Chem B* 2003;107:7540–3.
- [40] Strickler JH, Webb WW. Three-dimensional optical data storage in refractive media by two-photon point excitation. *Opt Lett* 1991;16:1780–2.
- [41] Cammi R, Cossi M, Tomasi J. Analytical derivatives for molecular solutes. III. Hartree-Fock static polarizability and hyperpolarizabilities in the polarizable continuum model. *J Chem Phys* 1996;104:4611–20.
- [42] Shen YR. The principles of nonlinear optics. New York: Wiley; 1984.
- [43] GAUSSIAN 03, References in <http://www.gaussian.com>.
- [44] Olsen J, Jorgensen P. Linear and nonlinear response functions for an exact state and for an MCSCF state. *J Chem Phys* 1985;82:3235–64.
- [45] DALTON, a molecular electronic structure program, Release Dalton. see, <http://daltonprogram.org/>; 2011.